Observation of Zero-Field Transverse Resistance in AlO_x/$SrTiO_3$ Interface Devices

P. W. Krantz⬤ and V. Chandrasekhar

Department of Physics, Northwestern University, Evanston, Illinois 60208, USA

Domain walls in AlO_x/$SrTiO_3$ (AlO_x/STO) interface devices at low temperatures give a rise to a new signature in the electrical transport of two-dimensional carrier gases formed at the surfaces or interfaces of STO-based heterostructures: a finite transverse resistance observed in Hall bars in zero external magnetic field. This transverse resistance depends on the local domain wall configuration and hence changes with temperature, gate voltage, thermal cycling, and position along the sample and can even change sign as a function of these parameters. The transverse resistance is observed below $\simeq 70$ K but grows and changes significantly below $\simeq 40$ K, the temperature at which the domain walls become increasingly polar. Surprisingly, the transverse resistance is much larger in (111) oriented heterostructures in comparison to (001) oriented heterostructures. Measurements of the capacitance between the conducting interface and an electrode applied to the substrate, which reflect the dielectric constant of the STO, indicate that this difference may be related to the greater variation of the temperature-dependent dielectric constant with electric field when the electric field is applied in the [111] direction. The finite transverse resistance can be explained inhomogeneous current flow due to the preferential transport of current along domain walls that are askew to the nominal direction of the injected current.

Two-dimensional carrier gases (2DCGs) in $SrTiO_3$ (STO)-based interface devices show a variety of complex correlated electron phenomena, including superconductivity [1–3], magnetism [4–8], and strong spin-orbit interactions [3,9,10]. These phenomena are tunable with an electric field, typically applied by means of a voltage V_g applied to the STO substrate, which convolutes the gating effects with the rather complex dielectric properties of STO [11–14]. Recently, it has been recognized that the domain walls formed between tetragonal domains in the low-temperature phase of STO play an important role in determining the properties of 2DCGs in STO-based devices [15–24]. Here we show that these domain walls give rise to a new effect at low temperatures: a finite transverse resistance observed in AlO_x/STO Hall bars at low temperatures in zero external magnetic field. The transverse resistance depends on the local domain wall configuration and hence can change with temperature, gate voltage, thermal cycling, and position along the sample. Our results can be explained by inhomogeneous current flow due to the preferential transport of current along domain walls that are not collinear with the nominal direction of the injected current.

STO is a band gap insulator with a dielectric constant ϵ of a few hundred at room temperature that rises to a few tens of thousands at low temperatures (<20 K). This increase in ϵ is associated with an incipient displacive ferroelectricity that is frustrated by quantum fluctuations, the so-called quantum paraelectric transition that occurs around 40 K [12,15]. STO also undergoes a structural transition from a cubic to tetragonal phase with a slight change of the c axis at 105 K, forming domain walls between tetragonal domains with randomly oriented c axes. Dielectric spectroscopy shows that the domain walls may be polar [16,17], local imaging studies have shown that current through 2DCGs flows preferentially along the domain walls [23], and that these domain walls can also be magnetic [24]. As we show below, preferential charge transport along these domain walls gives rise to a finite zero-field transverse resistance (ZFTR) that increases in magnitude significantly below 40 K, near the quantum paraelectric transition of STO. Its characteristics indicate that it is sensitive to the formation and dynamics of domain walls in STO at low temperatures.

Measurements of the transverse resistance, where the voltage contacts are aligned perpendicular to the path of the current in a Hall bar geometry, are a powerful tool to obtain important information about the intrinsic properties of a material. In conventional conductors, the transverse resistance is an antisymmetric function of an externally applied magnetic field arising from the Hall effect. It depends on the sign, density, and mobility of the charge carriers, and as such, vanishes at zero magnetic field [25]. In materials with a finite magnetic moment, such as ferromagnets, there might be a component of the transverse resistance that is hysteretic with the applied field and has a nonvanishing contribution at zero applied field. The origin of this anomalous Hall effect arises from broken time-reversal symmetry in the presence of spin-orbit interactions [26]. In other cases, the role of time-reversal symmetry breaking is

not clear. For example, inhomogeneous current flow arising from defects [27] or anisotropy in the resistivity tensor [28] may also give rise to ZFTR without involving time-reversal symmetry breaking. We propose that a similar explanation describes our observations.

The samples in our experiments were fabricated by depositing Al in patterned Hall bar configurations on $5 \times 5 \times 0.5$ mm Ti-terminated STO substrates to form an amorphous AlO_x layer that pulled oxygen from the STO substrate, resulting in oxygen vacancies and a 2DCG at the AlO_x/STO interface. The Al was deposited in steps of 2 nm, each deposition followed by oxidation in a 100 mT oxygen environment without breaking vacuum. The Hall bars, each 600 μm long and 50 μm wide, were aligned along primary surface crystal directions: equivalent $\langle 100 \rangle$ directions for the (001) STO substrate, and $[\bar{1}\,\bar{1}\,2]$ and $[1\bar{1}0]$ surface crystal directions for the (111) STO substrate. In addition to the longitudinal resistance R_L, the sample geometry permitted measurements of two transverse resistances R_T [Figs. 1(a) and 1(b)]. Resistance measurements of the Hall bars and capacitance measurements between the Hall bars and the back gate were performed as a function of temperature T, back gate voltage V_g, and magnetic field B in a liquid helium cryostat equipped with a superconducting magnet. The resistance measurements were performed using lock-in amplifier techniques at low frequency using a custom-built current source. Capacitance measurements were performed by superposing a 1 kHz ac voltage on the dc gate voltage V_g and measuring the current generated in the Hall bar, as described in Ref. [29].

As with other STO-based 2DCGs, the transport properties of the devices can be tuned by an electric field applied by means of a gate voltage to the substrate. Applying a finite gate voltage V_g at low temperature irreversibly changes the properties of the 2DCG so that the initial resistance at $V_g = 0$ V cannot be recovered unless the sample is warmed up to room temperature before cooling back down. This phenomenon is well known in STO-based oxide interfaces [30]. For this reason, we discuss below only data as V_g was progressively increased from 0 to 80 V. Sweeping back down in V_g, in general, results in larger values of resistance at the same value of V_g, but the qualitative results do not change. Sheet resistances at ~5 K and $V_g = 0$ V were $R_\square \sim 500$ Ω and $R_\square \sim 750$ Ω for the (001) and (111) Hall bars, respectively, with the corresponding areal charge densities of $n \sim 9 \times 10^{13}$/cm^2 and $n \sim 2 \times 10^{13}$/cm^2 (see Supplemental Material [31]).

Figures 1(c) and 1(d) show representative longitudinal (R_L) and transverse (R_T) resistances of Hall bars on (001) and (111) oriented samples as a function of temperature at $V_g = 80$ V and $B = 0$. A finite R_T is seen in both orientations, with the magnitude of R_T in the (111) Hall bars being much larger in comparison to the (001) Hall bars. Care was taken to qualify the sample geometry and alignment, as a finite R_T in zero field is most commonly attributed to misalignment of the transverse voltage probes, so that some fraction of R_L contributes to R_T. If so, one would expect R_T to track R_L as a function of temperature. The data in Figs. 1(c) and 1(d) show that this is not the case for these devices. A more detailed discussion of the
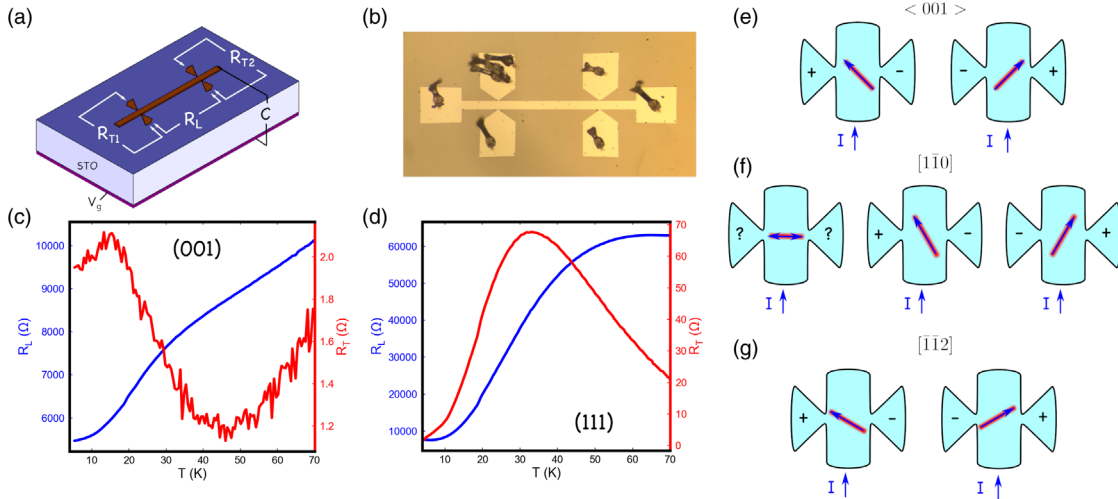

FIG. 1.   (a) Schematic of a Hall bar, showing the voltage probes used to measure the longitudinal (R_L) and transverse (R_T) resistances and the capacitance C. The gate voltage V_g is applied to the back of the STO substrate. (b) Optical image of a Hall bar. Temperature dependence of R_L (blue) and R_T (red) for a (c) (001) oriented Hall bar and a (d) (111) Hall bar, for $V_g = 80$ V and $B = 0$. (e)–(g) Schematic representation of orientation of domain walls near transverse voltage probes. Red lines represent domain walls, and blue represents current direction along these domain walls. (e) [001] oriented sample, with injected current direction along the $\langle 001 \rangle$ surface crystal directions. (f),(g) [111] oriented sample with the current injected along the (f) $[1\bar{1}0]$ direction and along the (g) $[\bar{1}\,\bar{1}\,2]$ direction. The third wall in (g) would be oriented parallel to the injected current and is therefore not shown.
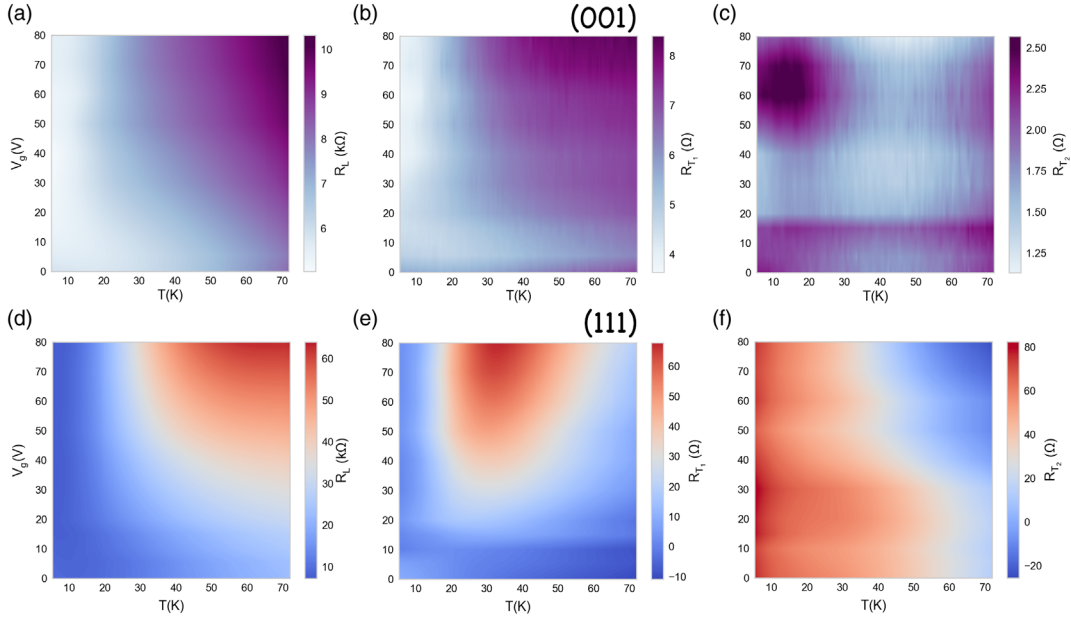
FIG. 2. (a)–(c) Gate voltage and temperature dependence at $B = 0$ of the longitudinal resistance R_L and two transverse resistances R_{T_1} and R_{T_2} for a (001) oriented Hall bar. (d)–(f) Corresponding data for a (111) oriented Hall bar.

possible sources of transverse signal can be found in the Supplemental Material [31].

Figure 2 shows the full temperature and gate voltage dependence of the longitudinal resistance R_L and the two transverse resistances R_{T_1} and R_{T_2} [see Fig. 1(a)] for both a (001) and a (111) oriented Hall bar at $B = 0$. There are a number of features of these data that should be noted (these features are reproduced in all the Hall bars we have measured). First, R_L for both the (001) and the (111) oriented samples has its lowest value at low T and small values of V_g, and its highest value at $V_g = 80$ V and high T. While R_L at high T and large V_g is about a factor of 6 larger for the (111) sample in comparison to the (001) sample, R_L at low T and small V_g for the two Hall bars is comparable. Second, the change in R_{T_1} and R_{T_2} over the range of V_g and T shown is larger by a factor of 20 or more for the (111) sample in comparison to the (001) sample. Third, for both (001) and (111) Hall bars, the two transverse resistances R_{T_1} and R_{T_2} measured at points 600 μm apart on the same Hall bar are qualitatively different from each other in their dependence on T and V_g. Finally, R_T can change sign as a function of T or V_g for both the (001) and the (111) oriented samples. An example of this for the (111) sample can be seen in Figs. 2(e) and 2(f).

In addition to varying spatially along the length of a single Hall bar, R_T in zero field also changes quantitatively and qualitatively after warming the sample to room temperature and cooling back down again, even though R_L may not change. This is shown in Figs. 3(a) and 3(b), which show the simultaneously measured zero-field R_T and R_L for two different (111) oriented devices on two separate cooldowns after warming to room temperature. In both

measurements, R_L remains unchanged, but the transverse resistance R_T varies by 40% or more at low temperatures. Furthermore, letting the sample anneal at room temperature for several days can change R_L due to a change in the oxygen vacancy concentration and cause dramatic changes to the analytic shape of R_T. It may initially show behavior similar to Fig. 2(e), but then show a change in resistance, as in Fig. 2(f), on a subsequent cooldown. The differences in R_T measured from the same set of probes are accentuated below 40 K, but converge to roughly the same value at higher temperatures, as can be seen from Figs. 3(a) and 3(b).

Recent experimental studies [20–23] have shown that current in STO-based 2DCGs appears to flow preferentially along the domain walls formed between tetragonal domains. The domain walls form along the {110} planes [34] and range from a few microns to many tens of microns in length. They are aligned at specific angles to the nominal direction of the injected current in our devices, as shown in Figs. 1(e)–1(g). For the Hall bars on the (001) oriented substrates, these angles are $\pm 45°$, while for the Hall bars on the (111) oriented substrates, the angles are $\pm 30°$ and $90°$ for Hall bars aligned along the $[1\bar{1}0]$ surface crystal direction and $\pm 60°$ and $0°$ for Hall bars aligned along the $[\bar{1}\,\bar{1}\,2]$ surface crystal direction. Current flow along these domain walls would give rise to finite off-diagonal components of the resistivity tensor (ρ_{xy}, ρ_{yx}) that vary as a function of position, as they depend on the local domain configuration. Since the domain configuration is random, and the current is equally likely to be deflected to the right or to the left, the sign of the resulting transverse resistance can be positive or
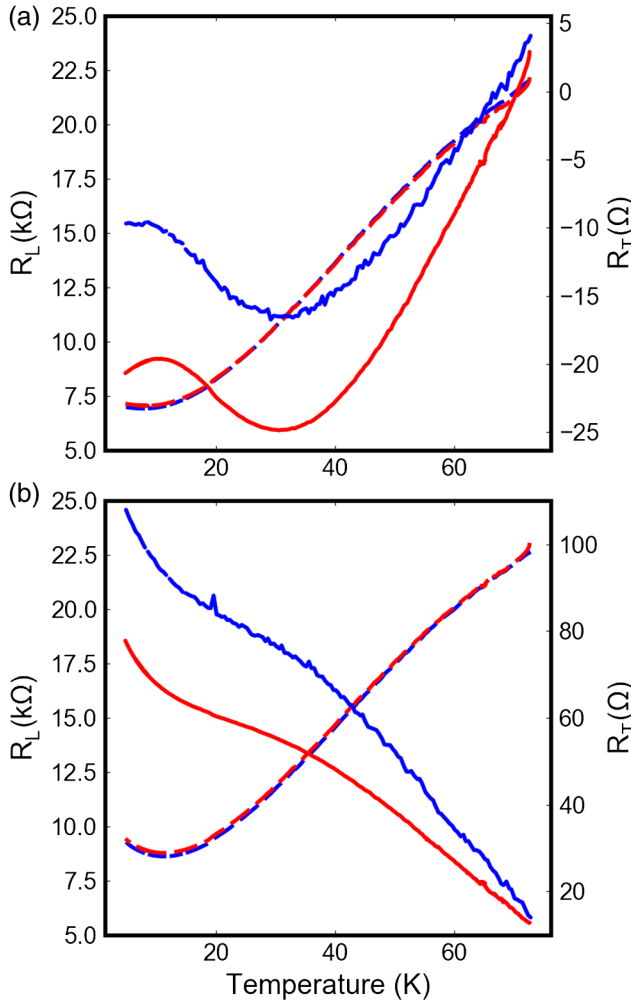
FIG. 3. (a) Red and blue solid curves show the transverse resistance R_T for $V_g = 0$, $B = 0$ for a (111) oriented sample on two different cooldowns. The dashed curves show the corresponding simultaneously measured longitudinal resistance R_L. (b) Similar data for a different (111) oriented Hall bar.
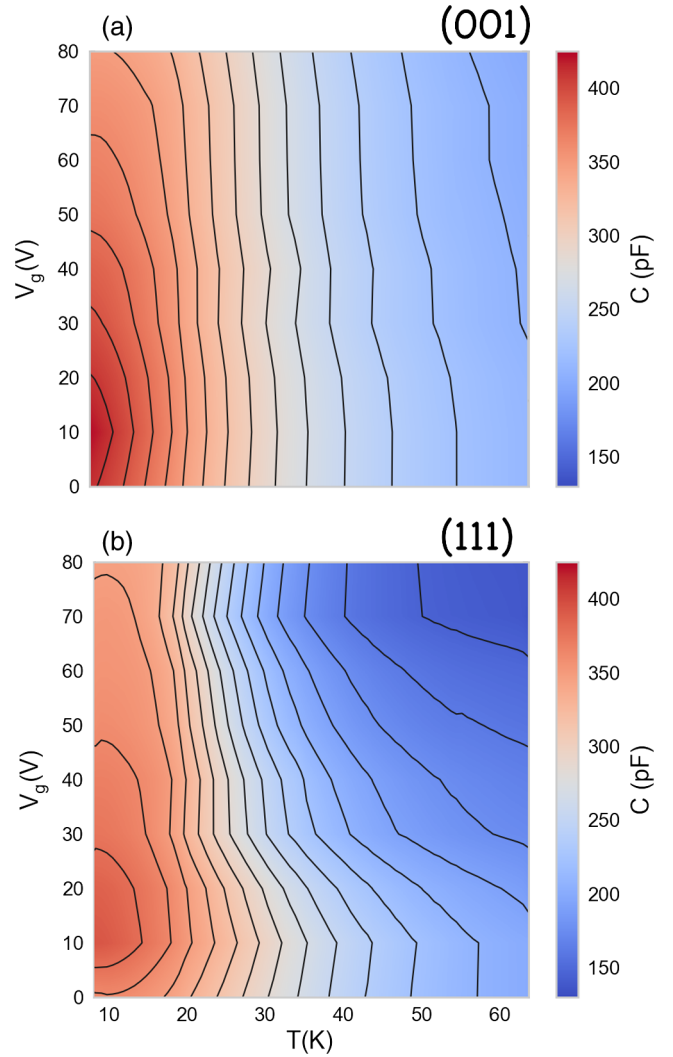

FIG. 4. Temperature and gate voltage dependence of capacitance. (a) Capacitance measured between the back gate and a Hall bar on a [001] oriented substrate as a function of T and V_g. (b) Similar data for a (111) oriented Hall bar.

negative, as shown in Figs. 1(e)–1(g). Consequently, for very wide samples encompassing many such domain walls, one might expect the transverse resistance to average to zero, while for narrower devices with only one or a few domain walls, the effect would be larger. The domain walls are known to reconfigure on thermal cycling and move under the influence of a back gate voltage [19–21,34]. They are also reported to become more polar at temperatures below 40 K [17]. These properties are all consistent with the properties of the ZFTR, suggesting that charge transport along domain walls is responsible for the transverse resistance we observe. As previously noted, intrinsic magnetism may give rise to a ZFTR, but there were no signatures of magnetic order in longitudinal or Hall magnetoresistance traces (see Supplemental Material [31]).

Based on the model above, we would expect the magnitude of the ZFTR in the (001) and (111) oriented

samples to be the same. However, the magnitude of the change in the ZFTR as a function of T and V_g is much larger for the (111) oriented samples in comparison to the (001) oriented samples. In order to explore the potential reason for this difference, we measured the T and V_g dependence of the capacitance C between the Hall bars and the back gate [29]. Modeling the system as a parallel plate capacitor, C directly reflects the dielectric constant ϵ of the STO. These capacitance data are shown in Figs. 4(a) and 4(b) for a (001) and a (111) oriented Hall bar, respectively. For both orientations, C increases as T decreases, and at the lowest temperature, decreases with increasing V_g, consistent with previous measurements of ϵ in STO where the electric field was applied along the $\langle 100 \rangle$ or $\langle 110 \rangle$ crystal directions [11–13]. However, there is a difference in the V_g dependence of $C(T)$ between the two orientations: For the (001) sample, $C(T)$ is not strongly

dependent on V_g, while for the (111) sample, there is a significant sharpening of the transition from low capacitance at higher temperatures to higher capacitance at lower temperatures with increasing V_g, with the transition region moving from approximately 30 K down to 20 K as V_g increases from 0 to 80 V. We note that earlier measurements [13] of the dielectric constant of STO have been performed with the electric field aligned along the $\langle 100 \rangle$ or $\langle 110 \rangle$ directions, and no significant differences between different field directions were noted. In the absence of polar domain walls, it is not immediately clear why the dielectric constant should depend on the direction of the electric field with respect to the crystalline axes, given that the c axes of tetragonal domains are randomly oriented along the $\langle 100 \rangle$ directions. The greater sensitivity of both the ZFTR and the capacitance of our structures when the electric field is aligned along the [111] direction suggests a common origin of dynamic domain walls for both effects.

In summary, we propose that preferential conduction along domain walls is responsible for the zero-field transverse resistance observed in our AlO_x/STO samples. The effect is primarily a function of electric field, temperature, and crystal direction, but is also subject to the dynamics of domain formation in the STO. Capacitance measurements conducted to probe the difference in sample crystal orientation revealed a directional dependence of the dielectric constant and suggest a common origin around the quantum paraelectric transition. These results have significant implications for making mesoscopic devices from STO-based oxide heterostructures, especially those on [111] substrates.

[1] N. Reyren, S. Thiel, A. D. Caviglia, L. F. Kourkoutis, G. Hammerl, C. Richter, C. W. Schneider, T. Kopp, A.-S. Rüetschi, D. Jaccard, M. Gabay, D. A. Muller, J.-M. Triscone, and J. Mannhart, Superconducting interfaces between insulating oxides, Science 317, 1196 (2007).

[2] A. D. Caviglia, S. Gariglio, N. Reyren, D. Jaccard, T. Schneider, M. Gabay, S. Thiel, G. Hammerl, J. Mannhart, and J.-M. Triscone, Electric field control of the LaAlO$_3$/SrTiO$_3$ interface ground state, Nature (London) 456, 624 (2008).

[3] M. B. Shalom, M. Sachs, D. Rakhmilevitch, A. Palevski, and Y. Dagan, Tuning Spin-Orbit Coupling and Superconductivity at the SrTiO$_3$/LaAlO$_3$ Interface: A Magnetotransport Study, Phys. Rev. Lett. 104, 126802 (2010).

[4] M. Huijben, A. Brinkman, G. Koster, G. Rijnders, H. Hilgenkamp, and D. H. A. Blank, Structure-property relation of SrTiO$_3$/LaAlO$_3$ interfaces, Adv. Mater. 21, 1665 (2009).

[5] D. A. Dikin, M. Mehta, C. W. Bark, C. M. Folkman, C. B. Eom, and V. Chandrasekhar, Coexistence of

[6] J. A. Bert, B. Kalisky, C. Bell, M. Kim, Y. Hikita, H. W. Hwang, and K. A. Moler, Direct imaging of the coexistence of ferromagnetism and superconductivity at the LaAlO$_3$/SrTiO$_3$ interface, Nat. Phys. 7, 767 (2011).

[7] L. Li, C. Richter, J. Mannhart, and R. Ashoori, Coexistence of magnetic order and two-dimensional superconductivity at LaAlO$_3$/SrTiO$_3$ interfaces, Nat. Phys. 7, 762 (2011).

[8] M. Mehta, D. A. Dikin, C. W. Bark, C. M. Folkman, C. B. Eom, and V. Chandrasekhar, Hysteretic Hall resistance at the LaAlO$_3$-SrTiO$_3$ interface: Interplay between superconducting and ferromagnetic properties, J. Phys. Conf. Ser. 400, 022071 (2012).

[9] A. D. Caviglia, M. Gabay, S. Gariglio, N. Reyren, C. Cancellieri, and J. M. Triscone, Tunable Rashba Spin-Orbit Interaction at Oxide Interfaces, Phys. Rev. Lett. 104, 126803 (2010).

[10] V. V. Bal, Z. Huang, K. Han, Ariando, T. Venkatesan, and V. Chandrasekhar, Strong spin- orbit coupling and magnetism in (111) (La$_{0.3}$Sr$_{0.7}$)(Al$_{0.65}$Ta$_{0.35}$)O$_3$/SrTiO$_3$, Phys. Rev. B 98, 085416 (2018).

[11] H. E. Weaver, Dielectric properties of single crystals of SrTiO$_3$ at low temperatures, J. Phys. Chem. Solids 11, 274 (1959).

[12] K. A. Müller and H. Burkard, SrTiO$_3$: An intrinsic quantum paraelectric below 4 K, Phys. Rev. B 19, 3593 (1979).

[13] K. A. Müller, W. Berlinger, and E. Tosatti, Indication for a novel phase in the quantum paraelectric regime of SrTiO$_3$, Z. Phys. B 84, 277 (1991).

[14] S. E. Rowley, L. J. Spalek, R. P. Smith, M. P. M. Dean, M. Itoh, J. F. Scott, G. G. Lonzarich, and S. S. Saxena, Ferroelectric quantum criticality, Nat. Phys. 10, 367 (2014).

[15] P. Chandra, G. G. Lonzarich, S. E. Rowley, and J. F. Scott, Prospects and applications near ferroelectric quantum phase transitions: A key issues review, Rep. Prog. Phys. 80, 112502 (2017).

[16] J. F. Scott, E. K. H. Salje, and M. A. Carpenter, Domain Wall Damping and Elastic Softening in SrTiO$_3$: Evidence for Polar Twin Walls, Phys. Rev. Lett. 109, 187601 (2012).

[17] E. K. H. Salje, O. Aktas, M. A. Carpenter, V. V. Laguta, and J. F. Scott, Domains Within Domains and Walls Within Walls: Evidence for Polar Domains in Cryogenic SrTiO$_3$, Phys. Rev. Lett. 111, 247603 (2013).

[18] J. Fontcuberta, V. Skumryev, V. Laukhin, X. Granados, and E. K. H. Salje, Polar domain walls trigger magnetoelectric coupling, Sci. Rep. 5, 13784 (2015).

[19] H. J. H. Ma, S. Scharinger, S. W. Zeng, D. Kohlberger, M. Lange, A. Sthr, X. R. Wang, T. Venkatesan, R. Kleiner, J. F. Scott, J. M. D. Coey, D. Koelle, and Ariando, Local Electrical Imaging of Tetragonal Domains and Field-Induced Ferroelectric Twin Walls in Conducting SrTiO$_3$, Phys. Rev. Lett. 116, 257601 (2016).

[20] Y. Frenkel, N. Haham, Y. Shperber, C. Bell, Y. Xie, Z. Chen, Y. Hikita, H. Y. Hwang, and B. Kalisky, Anisotropic transport at the LaAlO$_3$/SrTiO$_3$ interface explained by microscopic imaging of channel-flow over SrTiO$_3$ domains, ACS Appl. Mater. Interfaces 8, 12514 (2016).

[21] Y. Frenkel, N. Haham, Y. Shperber, C. Bell, Y. Xie, Z. Chen, Y. Hikita, H. Y. Hwang, E. K. H. Salje, and B. Kalisky,

Imaging and tuning polarity at SrTiO$_3$ domain walls, Nat. Mater. **16,** 1203 (2017).

[22] N. J. Goble, R. Akrobetu, H. Zaid, S. Sucharitakul, M.-H. Berger, A. Sehirlioglu, and X. P. A. Gao, Anisotropic electrical resistance in mesoscopic LaAlO$_3$/SrTiO$_3$ devices with individual domain walls, Sci. Rep. **7,** 44361 (2017).

[23] B. Kalisky, E. M. Spanton, H. Noad, J. R. Kirtley, K. C. Nowack, C. Bell, H. K. Sato, M. Hosoda, Y. Xie, Y. Hikita, C. Woltmann, G. Pfanzelt, R. Jany, C. Richter, H. Y. Hwang, J. Mannhart, and K. A. Moler, Locally enhanced conductivity due to the tetragonal domain structure in LaAlO$_3$/SrTiO$_3$ heterointerfaces, Nat. Mater. **12,** 1091 (2013).

[24] D. V. Christensen, Y. Frenkel, Y. Z. Chen, Y. W. Xie, Z. Y. Chen, Y. Hikita, A. Smith, L. Klein, H. Y. Hwang, N. Pryds, and B. Kalisky, Strain-tunable magnetism at oxide domain walls, Nat. Phys. **15,** 269 (2019).

[25] J. M. Ziman, *Theory of Solids*, 2nd ed. (Cambridge University Press, Cambridge, England, 1972).

[26] N. Nagaosa, J. Sinova, S. Onoda, A. H. MacDonald, and N. P. Ong, Anomalous Hall effect, Rev. Mod. Phys. **82,** 1539 (2010).

[27] V. LaukhinL. Abad, B. Martínez, J. Fontcuberta, O. Gorbenko, and A. Kaul, Transverse resistance measurements: A very sensitive probe to charge inhomogeneities in manganites, J. Phys. D **37,** 3145 (2004).

[28] J. Wu, A. T. Bollinger, X. He, and I. Bożović, Spontaneous breaking of rotational symmetry in copper oxide superconductors, Nature (London) **547,** 432 (2017).

[29] S. Davis, V. Chandrasekhar, Z. Huang, K. Han, Ariando, and T. Venkatesan, Anisotropic multicarrier transport at the (111) LaAlO$_3$/SrTiO$_3$ interface, Phys. Rev. B **95,** 035127 (2017).

[30] J. Biscaras, S. Hurand, C. Feuillet-Palma, A. Rastogi, R. C. Budhani, N. Reyren, E. Lesne, J. Lesueur, and N. Bergeal, Limit of the electrostatic doping in two-dimensional electron gases of LaXO$_3$ ($X =$ Al, Ti)/SrTiO$_3$, Sci. Rep. **4,** 6788 (2014).

[31] See Supplemental Material at http://link.aps.org/supplemental/10.1103/PhysRevLett.127.036801 for a detailed discussion of potential sample inhomogeneities, magnetoresistance measurements, and carrier density calculations, which includes Refs. [29,32,33].

[32] D. Pesquera, M. A. Carpenter, and E. K. H. Salje, Glasslike Dynamics of Polar Domain Walls in Cryogenic SrTiO$_3$, Phys. Rev. Lett. **121,** 235701 (2018).

[33] A. Raslan, P. Lafleur, and W. A. Atkinson, Temperature-dependent band structure of SrTiO$_3$ interfaces, Phys. Rev. B **95,** 054106 (2017).

[34] M. Honig, J. A. Sulpizio, J. Drori, A. Joshua, E. Zeldov, and S. Ilani, Local electrostatic imaging of striped domain order in LaAlO$_3$/SrTiO$_3$, Nat. Mater. **12,** 1112 (2013).